CrossMark

Thermal structure of a major crustal shear zone, the basal thrust in the Scandinavian Caledonides

J. Fauconnier [a,b,*], L. Labrousse [a,b], T.B. Andersen [c], O. Beyssac [d], S. Duprat-Oualid [e], P. Yamato [e]

[a] UPMC Univ. Paris 06, UMR 7193, ISTeP, F-75005 Paris, France
[b] CNRS, UMR 7193, ISTeP, F-75005 Paris, France
[c] Center for Earth Evolution and Dynamics (CEED), Univ. of Oslo, Postbox 1047, Blindern, N-0316 Oslo, Norway
[d] Institut de Minéralogie et de Physique des Milieux Condensés (IMPMC), UMR CNRS-UPMC, Campus Jussieu, Case Courrier 115, 4 place Jussieu, F-75005 Paris, France
[e] Géosciences Rennes, CNRS UMR 6118, Université de Rennes 1, F-35042 Rennes, France

A R T I C L E   I N F O

A B S T R A C T

Crustal-scale thrust zones accommodate most of the horizontal shortening at the front of orogenic wedges. Their thermal state is a key feature of collision zones, depending on critical parameters such as thrust rate or initial thermal properties of involved lithosphere units. We present here the first direct imaging of the thermal envelope of such a thrust zone: the Jotun Basal Thrust (JBT) in the Scandinavian Caledonides, through Raman Spectroscopy of Carbonaceous Material in the alum shales, an organic carbon-rich unit of Cambro-Ordovician age along which the basal decollement of the JBT developed. Maximum temperature mapping within this unit shows isotherms grading from $\sim 320\,°C$ in the south–east to $\sim 500\,°C$ in the north–west in the trailing end of the nappe stack. Based on bt + chl + grt + ph equilibrium, we estimate that the trailing end reached a temperature of $500\,°C$ at 1.2 ± 0.1 GPa pressure. 2-D thermo-kinematic modelling constrained with these new natural data and timing considerations for the Scandian collision indicates that (1) peak temperature mainly reflects maximum burial stage, (2) thrust rate and dip angle must have been low for the JBT and (3) the Scandinavian Caledonides represent a relatively cold orogenic wedge compared to other orogens.

© 2013 Elsevier B.V. All rights reserved.

1. Introduction

In continental collision, most of the convergence between the facing plates is accommodated on a major thrust system at crustal to lithospheric scale. Our understanding of such crustal scale thrusts essentially comes from the well-studied and active Himalayan system (i.e. Main Frontal, Main Boundary and Main Central Thrusts) as well as the ancient equivalents such as the fold-and-thrust systems in the central and southern Appalachians (Boyer and Elliott, 1982). Numerical and analytical models on the thermal evolution of the MCT and the underthrusted Lesser Himalaya have been constrained by pressure–temperature paths or maximum temperature patterns across the MCT (Bollinger et al., 2004; Henry et al., 1997). Geometry at depth deduced from reflection and refraction seismic coupled with gravity measurements (Hetényi et al., 2006; Nábělek et al., 2009; Zhao et al., 1993) show that all thrusts branch from a shallowly dipping reverse ductile shear zone, the Main Himalayan Thrust (MHT), in which temperatures are only indirectly known.

The Scandinavian Caledonides, have many similarities to the Himalayas in both tectonostratigraphy and structure (Andersen et al., 2002; Labrousse et al., 2010) and therefore provide a unique opportunity to study the deeper parts of a crustal-scale thrust that compares with the MHT in size and offset. The Jotun Basal Thrust (JBT) accommodated a significant portion of the relative motion between the Caledonian nappe stack and in-situ basement and cover of Baltica during the Scandian collision and its later collapse (Andersen, 1998; Fossen and Dunlap, 1998). The late Proterozoic to lower Palaeozoic cover of the Baltic Shield, and most notably the graphitic black alum shale of late Cambrian to early Ordovician age, served as a decollement horizon for the thrusting. This carbon-rich black shale thus recorded the complete thermal evolution of the JBT. The thermometer based of Raman Spectrometry on Carbonaceous Material (RSCM, Beyssac et al., 2002) applied to the alum shales has enabled us to measure and map the peak temperatures along the thrust plane. Conventional thermobarometry and time-constraints from the Scandian orogeny sequence are used in the set-up of thermo-kinematic models for the JBT. The effect of convergence rate, thrust plane geometry, and duration of extensional reactivation are also evaluated. Synthetic thermal profiles from the

numerical models are then discussed in the light of our new natural data.

2. Geological setting

2.1. Caledonian tectonics

The basal thrust of the Scandinavian Caledonides developed as a crustal scale shear zone when the mountain belt was assembled during the collision between Baltica and Laurentia, known as the Scandian Orogeny (Gee, 1975). The resulting Scandian nappe-pile contains four main Allochthons (Lower, Middle, Upper and Uppermost) that can be traced along the exposed length (∼ 1800 km) of the orogen (Roberts and Gee, 1985). The Upper and Uppermost Allochthons are interpreted to be outboard oceanic terranes and portions of the overriding Laurentian plate, respectively (e.g. Roberts, 2003). The Middle- and Lower Allochthons are considered as the shortened pre-Caledonian passive to hyperextended margin of Baltica, but the Middle Allochthon may also contain some outboard exotic elements emplaced by large-scale strike-slip prior to the final collision (Nystuen et al., 2008; Andersen et al., 2012; Corfu et al., 2011; Kirkland et al., 2008).

In southern Scandinavia, the Middle Allochthon including the Jotun nappe is dominated by very large crystalline nappes of Proterozoic rocks, partly with meta-sedimentary cover (e.g. Lundmark and Corfu, 2007; Nystuen et al., 2008). In addition, an allochthonous melange unit with numerous mantle peridotites representing the remnants of deep basin(s) formed by hyperextension in the pre-Caledonian continental margin of Baltica, sits between the continental Lower Allochthon dominated by meta-sediments and the large Middle Allochthon nappes (see above and Andersen et al., 2012). The Jotun nappe is described as an association of Precambrian metamorphic basement thrust together with silico-clastic cover units ("Valdres Sparagmites") on top of the lower allochthon phyllites (Bryhni and Sturt, 1985).

The main thrusting of nappes onto Baltica started after the Middle Silurian Iapetus Ocean had closed in the Middle Silurian (∼ 430 Ma, e.g., Corfu et al., 2006; Torsvik and Cocks, 2005). Several Pre-Scandian events affected distal parts of the margin of Baltica prior to the final closure, at 482, 450 and 446 Ma (e.g. Andersen et al., 1998; Brueckner and van Roermund, 2004; Roberts, 2003; Root and Corfu, 2012). The onset of collision is dated at ∼ 430 Ma by: (i) cessation of subduction-related magmatism (e.g. Corfu et al., 2006), (ii) obduction of marginal basin/island-arc ophiolites in the Middle Silurian (Andersen and Jamtveit, 1990; Furnes et al., 1990) and (iii) the onset of the high-pressure metamorphism in the basement of Baltica (e.g. Glodny et al., 2008; Jolivet et al., 2005) as well as onset of molasses-type sedimentation in the foreland (Bockelie and Nystuen, 1985). The Scandian collision, crustal thickening and emplacement of the growing nappe-pile onto Baltica continued for ∼ 25 Myr during the early Devonian. The basement rocks of the Western Gneiss Region (WGR) in the footwall of the Caledonian floor thrust reached high- and ultra-high pressure metamorphic conditions at ∼ 410 to 400 Ma (e.g. Hacker et al., 2010; Kylander-Clark et al., 2008; Krogh et al., 2011). At this stage the Caledonian mountain belt in Scandinavia and East-Greenland reached dimensions similar to those of the present-day Himalaya (Labrousse et al., 2010).

The extensional phase that follows convergence can be divided in two stages (Fossen, 1992; Andersen, 1998). The early phase (Mode-I in Fossen, 1992) was induced by crustal collapse and results in reactivation of the JBT as a detachment. Late extension (Mode-II) produced crustal-scale extensional shear zones such as the Hardanger–Lærdal–Gjende Fault Zone (HLGFZ), which cross-cuts the entire nappe pile (Fossen and Hurich, 2005).

2.2. The alum shales

The black shales of the JBT, here subject to RSCM study, are located immediately above a thin discontinuous sedimentary cover to the allochthonous basement of Baltica (Fig. 1a). The basal decollement is more specifically located in the mechanically weak, organic-rich alum shales of Late Cambrian to Early Ordovician age (e.g. Bruton et al., 2010). In the field the alum shales are commonly 1 to 100 m thick and very rich in carbonaceous material (CM), with a Total Organic Carbon (TOC) up to 15% (Gautneb and Saether, 2009). The floor thrust is underlain by a thin and discontinuous (para)autochthonous cover of shale, quartzite and dispersed pockets of mostly thin basal conglomerate (e.g. Bruton et al., 1989). The floor-thrust known as the 'Osen-Røa Detachment' in the foreland of SE Norway (e.g. Nystuen, 1981; Bruton et al., 2010), can be traced westward below the Allochthons, across south-central Norway and continues into the JBT (Fig. 1). The JBT and the underlying autochthon reappear within the line of prominent basement windows formed by post-Caledonian (Permo–Triassic and younger) faulting accompanied by footwall uplift along the HLGFZ (Fig. 1) in central south Norway and beyond (Andersen et al., 1990; Fossen, 2010). The primary basement-cover relationships with local preservation of depositional contacts have also been identified below the basal thrust zone and nappes along the SE-margin of the WGR between the Bergen Arcs and Lom (Lutro and Tveten, 1998; Milnes et al., 1997). The basal thrust of the Caledonian mountain belt in South Norway can consequently be traced almost continuously across the strike from the down-faulted pin-point in the foreland south–east of Oslo within the Oslo Rift, between the deformed series at Holmstrand and the flat-lying Cambro-Silurian at Langesund (Oftedahl, 1943 in Morley, 1986; Bruton et al., 2010), to the hinterland cover on the WGR, over a distance of approximately 250 km. Our sampling profiles were collected away from areas where local thermal effect of the large Permo-Carboniferous magmatic rocks of the Oslo Rift were identified from conodont colour alteration index (Aldridge, 1984), and hence cover only 150 km of the observable across-strike section 180 km away from the fossil front (Fig. 1).

Samples collected in this study (Table 1, Fig. 1) show penetrative ductile stretching (Fig. 1a) with lineations trend from 100° to 135°. The foliation is parallel to the JBT, dipping toward the SE or NW defining the limbs of a large-scale synform in South Norway. Shear bands, drag folds, asymmetric boudinage within the alum shales systematically indicate top to NW to W shear-senses (Fig. 2), except for 2 sampling sites preserving top to SE shear sense indicators (Fig. 1a). Most of the structures within the alum shale layer therefore reveal extension along the former JBT dip direction related to north-westward extensional reactivation of the JBT (Fossen, 1992; Andersen, 1998).

The age of deformation along the decollement post-dates deposition of the Late-Silurian molasse-type fluvial deposits in the foreland as well as Lower Devonian (408 Ma) thrust-related growth of muscovite dated by ^{40}Ar/^{39}Ar method near the extensional break-away of the Valdres area (Fossen and Dunlap, 1998). In the central part of the orogen the basal decollement as well as the meta-sedimentary thrust wedge were strongly affected by late- to post-orogenic NW-directed extension, which was partly contemporaneous with thrusting in the foreland (e.g. Andersen, 1998; Fossen, 2010). The latest ages on syn-kinematic muscovites in the Jotun nappe and the shallowest levels of the WGR below the JBT indicate a north-westward reactivation until 400 to 395 Ma (Fossen and Dunlap, 1998; Hacker, 2007). JBT therefore underwent some stretching during late Caledonian extension as well as normal offset along cross cutting extensional (Fossen and Hurich, 2005).

The JBT can therefore be considered as a crustal-scale structure that first accommodated thrusting of outer Baltican continental
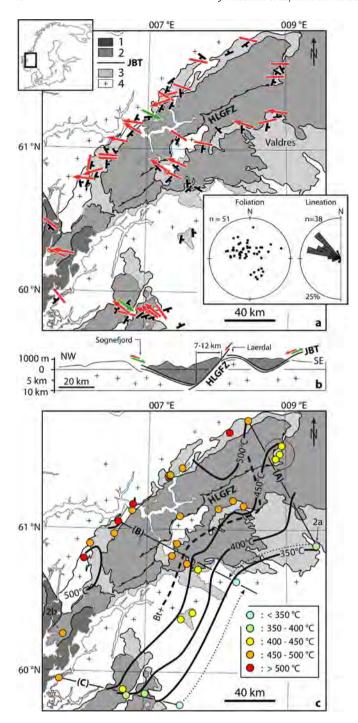
Fig. 1. (a) Location of sampling sites, foliation and lineation strike and dip. Arrows indicate sense of shear. Green arrows indicate syn-collisional thrust movements on JBT, red arrows indicate late top-to-northwest extension. Rose diagram shows lineations and stereoplot shows poles to foliation. 1. Upper Allochthon, 2. Middle Allochthon (i.e. Jotun nappe), 3. Lower Allochthon and Baltica cover, 4. Baltica basement. HLGFZ Hardanger–Lærdal–Gjende Fault Zone, JBT Jotun Basal Thrust. (b) Schematic cross-section through the southern Caledonides along profile B in Fig. 1c. Offset on the HLGFZ deduced from Lutro and Tveten (1998). (c) Maximum temperature estimates from RSCM on alum shales. A, B and C profiles refer to Fig. 3. Dashed arrows indicate the projection of profiles A and C on B for Fig. 3. Circled points are 46, 47, 48 discussed in the text. bt+ dashed line is biotite isograd.

margin as well as outboard terranes onto Baltica during Scandian collision for 25 Myr from 430 to 405 Ma (green arrows on Fig. 1a & b), which brought the westernmost WGR to UHP at 3.4 GPa (Hacker et al., 2010). Thereafter, it was reactivated as a top-to-west extensional detachment (red arrows on Fig. 1a & b) for 5 to 10 Myr

(from 405 to 400–395 Ma). In the studied section of southern Norway, the alum shale is a nearly continuous lithology within the decollement, recording its complete thermal evolution down-dip for 150 km parallel to its displacement direction.

3. RSCM temperature envelope of the JBT and constraints on its geometry

3.1. Method

Organic matter trapped in sediments gradually changes its chemistry and structure under the effect of heating, burial and subsequent metamorphism (Beyssac et al., 2002). The RSCM thermometry is based on the quantitative determination of the degree of graphitisation of CM which is a reliable indicator of metamorphic temperature. Because graphitisation of CM is irreversible, the structural modification recorded by Raman spectrometry is insensitive to retrogression and therefore records the maximum temperature experienced by the rocks during a PT-time loop (Beyssac et al., 2002). Temperature can be determined with absolute confidence of $\pm 50\,^{\circ}$C in the range 330–650 $^{\circ}$C. Within-sample and relative uncertainties between samples are, however, much smaller, in the 10–15 $^{\circ}$C range (Beyssac et al., 2004). More recent work on lower-grade rocks have shown that CM Raman spectra also can be correlated with the metamorphic temperature in the range at 200–330 $^{\circ}$C and a systematic correlation of the Raman spectra and temperature expands the total range from 200 to 650 $^{\circ}$C (Lahfid et al., 2010). The absolute error of the method is $\pm 50\,^{\circ}$C, but we also estimate a standard deviation for each sample ($\sigma/\sqrt{n}$) which gives an insight on within-sample heterogeneity (detailed description of method and errors in Beyssac et al., 2002 and 2004). In this study Raman spectra were obtained using a Renishaw InVIA Reflex microspectrometer (IMPMC, Paris). We used a 514 nm Laser Physics argon laser in circular polarisation, and followed closely the analytical and fitting procedures described in Beyssac et al., (2002 and 2003). Measurements were done on polished thin sections and CM was systematically analysed below a transparent adjacent mineral, generally quartz. 586 spectra were recorded on 40 samples (Table 1) in extended scanning mode (700–2000 cm^{-1}, Fig. 2e) for lower T samples or restrained scanning mode (1200–1700 cm^{-1}, Fig. 2f) for higher T samples, with acquisition times from 30 to 60 seconds. Spectra were then processed using the software Peakfit (Beyssac et al., 2003).

3.2. Results

Temperatures were derived from 10 to 25 spectra in each sample. Only spectra disturbed by fluorescence of the adjacent mineral, and those measured in detrital graphite were not considered. Temperature estimates vary from 314 $^{\circ}$C to 515 $^{\circ}$C with a standard error between 2 and 7 (Table 1). Average scatter was $\pm 25\,^{\circ}$C with maximum value of $\pm 35\,^{\circ}$C. The low-T calibration values were preferred for 3 sites (1, 61 and 64), high-T calibration giving the same T values with larger scatters. In order to estimate the outcrop scale variations of maximum temperatures recorded by the alum shales, several outcrops were repeatedly sampled. Series 1a to 1d, or 9a and 9b coming from two outcrops yielded the same T_{max} value (Table 1) within the measurement uncertainties. Samples 92, 93 and 94 also come from the same outcrop. Differences in T_{max} are below 25 $^{\circ}$C, meaning local variations in carbonaceous material maturation are within uncertainties. It is therefore possible to interpret the 40 T_{max} estimates at the scale of the southern Caledonian nappes stack, as a mapping of the maximum temperatures reached by the alum shales along the footwall of the JBT during the Scandian collision (Fig. 1c). Along three profiles oriented perpendicular to the present-day thrust front, temperatures

Table 1

Samples, outcrop coordinates, mineral assemblages, number of spectra recorded for RSCM, R2 (*RA1) ratios calculated, average temperature and the standard deviation $\sigma/\sqrt{n}$.

Sample	Latitude	Longitude	Minerals	Raman			
				n spectra	R2 or RA1	T mean [°C]	$\sigma/\sqrt{n}$
1a	59.7570	7.5137	ph + pl	24	0.627*	314	3
1c				14	0.636*	325	2
1d				15	0.658*	353	2
4	59.8334	7.0139	chl + ph	16	0.584	381	2
6b	59.8176	6.7531	chl + ph + pl + tur	25	0.570	387	2
9a	59.8606	6.7008	ph + pl	15	0.504	417	2
9b				12	0.486	425	4
10b	59.9254	5.7898	cb + ph + pl	14	0.342	489	4
11	60.2419	5.8138	cb + chl + grt + ph + pl	15	0.355	483	4
16	60.7869	6.0705	bt + ph + pl	13	0.283	515	4
18	60.8942	6.1501	bt + cb + ph + pl + tur	15	0.386	469	4
20	61.0564	6.5500	bt + cb + chl + ph	13	0.284	515	5
21	61.1380	6.7509	bt + cb + ph	12	0.375	474	6
22	61.1819	6.7595	cb + chl + ph + pl	14	0.314	501	4
32	60.9693	6.4970	chl + ph	13	0.358	481	4
35	61.3760	7.2798	BT + chl + ph + pl	13	0.330	494	3
36	61.3831	7.2705	bt + chl + ph + pl	11	0.341	489	5
37	61.3886	7.2899	cb + ph + pl	18	0.349	485	4
38	61.3950	7.2843	bt + cb + ph	15	0.384	470	4
39	61.3964	7.3025	bt + ph + pl + tur	15	0.400	463	4
41	61.4459	7.4764	cb + chl + grt + ph	12	0.339	490	7
43	61.7041	8.1740	ph	14	0.242	534	4
44	61.7908	8.4500	chl + ph	15	0.329	495	4
46	61.6114	8.9519	ph	15	0.439	445	3
47	61.5518	8.9225	ph	13	0.464	435	3
48	61.5171	8.8619	chl + ph + tur	18	0.461	436	3
51	61.1808	8.3907	bt + cb + chl + ep + ph + pl	10	0.401	463	4
52	61.1581	8.0216	ph	15	0.366	478	5
54	61.1036	7.4560	bt + cb + chl + ph	15	0.343	488	4
56	60.9067	7.4221	bt + chl + ph + pl	13	0.366	478	6
57	60.8199	7.3539	bt + cb + chl + ph	15	0.412	458	3
58	60.7653	7.5740	ph	14	0.411	458	6
60	60.7259	7.7358	ph	16	0.458	437	3
61	60.6406	8.2944	ph	16	0.646*	338	3
62	60.3687	7.5015	chl + ph	14	0.431	449	3
63	60.4154	7.6679	ph + pl	14	0.460	436	7
64	60.8970	9.4593	–	13	0.658*	352	2
92	61.2186	8.2354	cb + chl + ph	14	0.418	455	2
93				14	0.382	471	3
94				14	0.361	480	4

rise from 314 to 352 °C in the SE end up to 483 to 534 °C at the NW termination (Fig. 3). The three profiles describe a regional increase in temperature with isotherms following the average strike of the Caledonian nappe-stack (Fig. 1c). When projected on a single profile (Fig. 3), our data show that temperature increase is roughly linear for the first 70 km from 320 °C to 500 °C. Temperature values for samples 46, 47 and 48 appear slightly out of trend on a temperature–distance diagram (circled in Figs. 1c and 3) possibly due to non-cylindricity of the regional tectonics toward the North. Alternatively it is also possible that these samples are from a structurally higher level, basement not being exposed near these sampling sites. Value points derived from samples in the hanging-wall of the HLGFZ have been restored in their initial position, considering horizontal offsets of 7 to 12 km on the HLGFZ according to cross-sections (Lutro and Tveten, 1998; Andersen et al., 1999), shaded boxes in Fig. 1b). Despite the offset on the HLGFZ, the samples in its hanging-wall do not show any changes in the global temperature trend. At regional scale, RSCM temperature pattern eventually draw a 130 km long subplanar envelope with lowest values of 320 °C at the present-day frontal hanging-wall cut off and 500 °C at the trailing end the JBT.

Corresponding with the maximum temperature increase, the alum shales also show a change in textural mode, from preserved detrital grains (micas, quartz and clay minerals) on the south–east (Fig. 2c), to chl + ph + pl + qz + CM ± cb paragenesis in the central area, and bt + ph + pl + qz + CM ± grt (Fig. 2d) in the trailing end near the WGR. The crystallization of biotite from chlorite can be traced as an isograd trending parallel to the nappe-stack regional strike between samples with comparable chemistries (Fig. 1c), close to the 450 °C RSCM isotherm.

Constraints on the maximum depth recorded by the alum shales were deduced from the peak metamorphic paragenesis bt + chl + grt + ph developed in the samples with highest RSCM temperatures. Within the paragenesis stability field in a pseudo-section derived from whole-rock composition of alum shales and thermodynamic modelling (supplemental material, Holland and Powell, 1998), Si content in phengites, reaching 3.2 Si p.f.u. and almandine rich ($X_{Alm} = 0.7$) overgrowth on garnet yield narrow PT conditions of 500–550 °C and 1.1–1.3 GPa pressures for peak equilibration, in agreement with the maximum temperature estimates from RSCM. Considering that this pressure corresponds a lithostatic pressure and assuming a density of 2700 kg/m³ in average for the crust, this PT estimate yields a 45 ± 4 km depth for the maximum burial of the north-westernmost studied shales/schists.
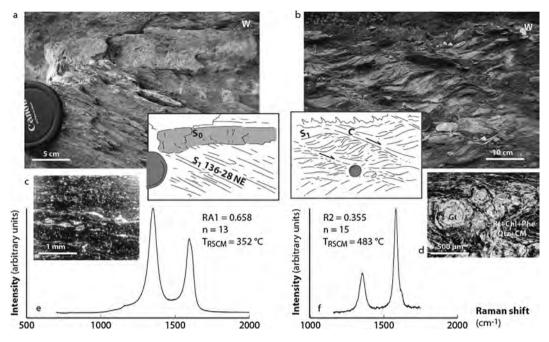
Fig. 2. Field photos, thin sections and representative Raman spectra for carbonaceous material from samples 64 (a, c, e) and 11 (b, d, f) (located 2a and 2b in Fig. 1) respectively on the southeastern and northwestern ends of profiles in Fig. 3. RA1 and R2 are parameters derived from curve fitting for low (Lahfid et al., 2010) and high (Beyssac et al., 2002) temperature calibrations.
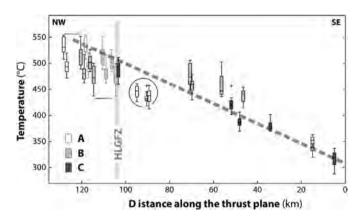

Fig. 3. RSCM temperatures profiles along lines A, B and C in Fig. 1. Segments represent maximum and minimum values, box plot represent 25%, 75% and median is shown within the box plots for each samples. Isolated cross stand for outliers. Shaded box-plots represent data points located in the hanging wall of the HLGFZ after restoration. Encircled points 46, 47, 48 are discussed in the text.

4. Thermo-kinematic modelling: the effect of convergence rate, dip and thermal heritage

The thermal profile along the JBT as deduced from RSCM data (Fig. 3) can be used as a constraint to model the thermal behaviour of a crustal scale thrust zone. The geodynamic significance of the maximum temperature profile remains unclear: is it representative of a synchronous stage in the JBT evolution or does it represent a diachronous envelope of its entire history? Once its significance is assessed, it can be used as a reference to evaluate the first order parameters governing the thermal profile shape of such a thrust zone. 2-D numerical modelling of temperature evolution along a thrust, both during collision and subsequent extensional reactivation, allowed us to test the influence of geometry, velocity and extensional reactivation on the maximal temperature distribution along the thrust, here considered as cylindrical (Fig. 1c).

4.1. Numerical code and experimental set-up

Relevant analytical computations of their thermal structure have been proposed for superficial wedge structures (e.g. Royden, 1993), as well as for lithospheric-scale thrust systems (Huw Davies and Stevenson, 1992). Nevertheless, integration of these partial analytical solutions would require interpolation (e.g. Huw Davies, 1999) for a full 2-D coverage of a complete orogenic wedge. For this reason, we privileged a numerical approach here, by using the thermo-kinematic model designed by Duprat-Oualid et al. (in press), to focus on the thermal evolution above and below crustal scale thrust systems. This code is an implicit finite difference code solving the heat equation (including diffusion, advection and heat production). The velocity field around the thrust is computed independently and the marker-in-cell method (Gerya, 2010) is used to advect temperature and rock properties through time. All the details about the numerical methods used in this study and comparisons with analytical solutions validating this code can be found in Duprat-Oualid et al. (in press).

Present-day topography in Western Norway, resulting of cumulated effects of N-Atlantic rifting (Redfield et al., 2005) and post-glacial uplift and erosion (Nielsen et al., 2009), is only poorly related to Caledonian tectonics. Estimates of climax Caledonian topography are based on comparison with Himalayas (Gabrielsen et al., 2005) or estimates of maximum crustal thickness (Andersen et al., 1998). Since no exact data is available for topography and erosion rates during the Caledonian collision, isostasy and erosion are not considered in this study. Shear heating, which in other studies have been shown to be important (e.g. Souche et al., 2013) is not included in the heat equation, since its implementation requires strong *a priori* hypothesis on parameters such as the effective viscosity of the shear zone, or the thickness on which strain is distributed. Furthermore the alum shale localizing the strain along the JBT has a very low shear strength and it is therefore unlikely that deformation produced significant heat (Souche et al., 2013).

Models are composed of three different horizontal layers as presented in Fig. 4: air (2 km), a 30 km thick continental crust, and a lithospheric mantle (Table 2) in a 150 km high model box.

Table 2
Parameters used for thermo-kinematic modelling of the JBT constant in every models presented.

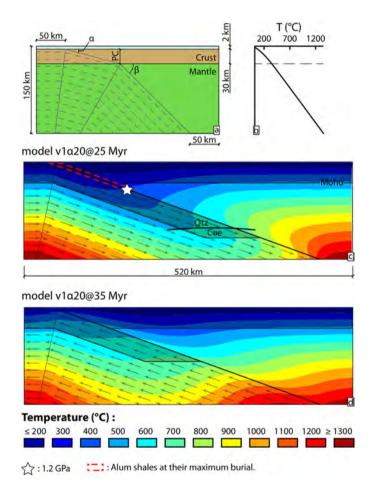| Parameter	Meaning	Value
dx and dz	Vertical and horizontal mesh resolution	2 km
H	Model height	150 km
H_c	Crust thickness	30 km
T_{surf}	Surface temperature	20 °C
Q_m	Basal heat flux	25×10^{-3} W m^{-2}
A	Surface radiogenic heat production	3×10^{-6} W m^{-3}
Z_r	Thickness of the radiogenic layer	10 km
ρ_c	Crust density	2700 kg m^{-3}
ρ_m	Mantle density	3300 kg m^{-3}
k	Thermal conductivity	3 W m^{-1} K^{-1}
Cp	Heat capacity	1000 J kg^{-1} K^{-1}

Fig. 4. Geometrical and velocity model setup (a). Geotherm used for the initial temperature field (b). Numerical model $v1\alpha20$ (i.e. 1 cm yr^{-1} convergence rate and 20° dipping thrust plane) geometry and isotherms pattern at maximum burial (c), and after 10 Myr divergence (d). White star pins depth where 1.2 GPa pressure is reached by the top of the subduction slab.

The width is adjusted so that 50 km remain on each side of the thrust whatever its dip to avoid side effects (Table 3 and Fig. 4). The spacial grid resolution is 2×2 km. Parameters such as density, thermal conductivity and heat capacity are not varied and are presented in Table 2. Radiogenic heat production is considered as exponential in the upper crust (10 km). Equivalent average radiogenic heat production for the upper crust would be 1.89 µW m^{-3} what compares with acknowledged average values for the continental crust (Rudnick and Gao, 2003). Thermal boundary conditions are set with constant surface temperature, constant basal heat flux (25 mW m^{-3}) and insulating boundary conditions (i.e. no heat flux) for the both lateral sides of the box. The initial geotherm is computed with a zero velocity field using the parameters described previously (i.e. constant surface temperature, constant heat flux, no heat flux on the side walls) until it reaches thermal equilibrium (i.e. a temperature change between two successive time-steps lower than 0.1 °C).

The duration of the thrusting is set to 25 Myr according to Scandian orogeny calendar (Section 2.1). Subduction dip angle and convergence rate are bound in order to bring the median continental crust to Ultra High Pressure (UHP) domain (100 km) at the end of continental subduction. In all models, subduction is followed by exhumation due to extension, with velocity equal to convergence rate.

Reference model ($v1\alpha20$) exhibits a 20° constant dip thrust with 1 cm yr^{-1} velocity (Table 3). Geometry effects have been explored by changing dip to 10° and velocity to 2 cm yr^{-1} in the experiment $v2\alpha10$. The effect of dip change within the mantle is evaluated in experiment $v1\alpha10\beta45$, with 10° superficial dip and 45° below 30 km, representing change from crustal to mantle lithologies and mechanical behaviour. The exhumation stage duration has been set to 10 Myr in the 3 configurations above, according to Scandian orogeny calendar. One experiment with 5 Myr lasting divergence ($v2\alpha10S$) evaluates the influence of a shorter extensional reactivation of the JBT, while $v2\alpha10L$ experiment represents a longer (20 Myr) extension scenario.

4.2. Results

All models show a deflection of isotherms (Fig. 4) during subduction stage, with temperature profile along the thrust zone flattening progressively from top to bottom with time. During divergence, profile turns convex upward, with inflexion point migrating from surface to depth with time (Fig. 5). The envelope profile resulting from this thermal evolution is therefore defined by the divergence stage at shallow depth and initial thermal conditions in the deeper part. This diachronous thermal envelope, representing the maximum temperature reached by markers at the top of the subducting slab, will later be compared with RSCM temperature estimates, considered as inherited from peak conditions (Fig. 6, Beyssac et al., 2002).

Thermal envelopes deduced from models, compare with peak thermal profiles computed for equivalent thrust zones (Fig. 7), Reference model $v1\alpha20$ is close to peak thermal profiles with equivalent set-up (model 1 in Henry et al., 1997, with no ero-

Table 3
Varying parameters for the different models. $v2\alpha10S$ and $v2\alpha10L$ are for short (5 Myr) and long-lasting (20 Myr) extensional reactivation.

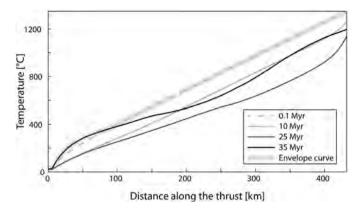| Model	Convergence rate, v [cm yr^{-1}]	First subduction angle, α [°]	Second subduction angle, β [°]	Dip changement depth, PC [km]	Exhumation duration, t [Myr]	Model width, W [km]
$v1\alpha20$	1	20			10	520
$v2\alpha10$	2	10			10	950
$v2\alpha10S$	2	10			5	950
$v2\alpha10L$	2	10			20	950
$v1\alpha10\beta45$	1	10	45	30	10	390

Fig. 5. Temperature profile along the thrust plane at 0.1, 10, 25, and 35 Myr for reference model $v1\alpha20$. Envelope curve of the instantaneous temperature profiles is used for comparison with RSCM data.
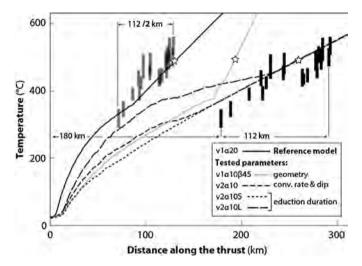

Fig. 6. Temperature profiles from numerical models and natural data. $v1$ series refer to models with 1 cm yr^{-1} convergence rate, $v2$ series to 2 cm yr^{-1}. α is the dip in degrees of the thrust at the surface, β is the second dip angle for slab with changing dip. S and L refer to models with shorter and longer extensional reactivation stages (5 and 20 Myr resp.). Natural data with their present-day position are shown with black rectangles. Grey rectangles show the same data with distances shortened by 50%. Stars represent the point along profiles where 1.2 GPa pressure was reached at maximum burial.

sion considered, mantle heat flux 28.5 mW m^{-2}, convergence rate 1.5 mm yr^{-1} and implementation of friction on fault). More sophisticated modelling with crustal layering, erosion and shear heating (Bollinger et al., 2006) also give similar results for a 20 Myr lasting activation. We therefore consider that our simplistic approach, even if not accounting for all processes occurring at depth, succeeds to reproduce first order thermal behaviour of subducting continental lithosphere. Along the reference profile for $v1\alpha20$ model, the 1.2 GPa pressure is reached at 130 km along the thrust. Convex shape is observed for the 100 shallower kilometers.

Change in dip and velocity from $v1\alpha20$ to $v2\alpha10$ causes a flattening of the temperature–distance profile along the thrust. 1.2 GPa pressure is reached at 250 km distance (Fig. 6). Thermal effect of divergence is observed for the 130 first kilometers. From reference model $v1\alpha20$ to $v1\alpha10\beta45$, the shape change induces a concave upward temperature profile, and 1.2 GPa pressure is reached at 190 km along the thrust. The effect of divergence is limited and restricted to the low temperature portion. Model $v2\alpha10S$ explores the effect of limited extensional stage. The resulting profile shows no convex portion in the first kilometers. Model $v2\alpha10L$ shows a wider (200 km long) convex portion with a maximum retrograde heating about 100 °C in comparison with model $v2\alpha10$.
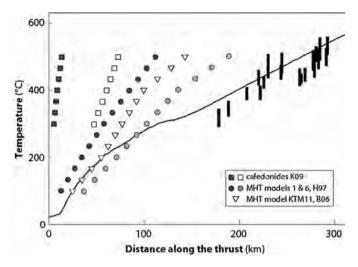

Fig. 7. Natural (black rectangles) and preferred synthetic profile (black line) from this study ($v2\alpha10$) compared to temperature profiles modelled for: the Caledonides (Kylander-Clark et al., 2009) at maximum burial (filled squares) and after 5 Myr exhumation of the upper lithosphere (open squares). Circles and triangles refer to the peak thermal state of the MHT in different thermo-kinematic models published by Henry et al. (1997) and Bollinger et al. (2006).

Diachronicity is therefore sensible only for long reactivation scenarios.

5. Discussion

The RSCM temperature estimates in the alum shales of the JBT throughout the Southern Scandinavian Caledonides yield a diachronous envelope for the thermal state of the shear zone during thrust and later extensional reactivation. Thermobarometry on the trailing end of the nappes allows to pin the now outcropping high T (500–520 °C) end of the alum shales unit at 1.2 GPa pressure, depth converted to a burial of 45 km. Assuming a cylindrical pattern for the RSCM temperature envelope, this can be rendered as a single profile to be compared with 2-D thermo-kinematic models for a crustal scale thrust zone. Rocks at the present-day hanging-wall cut-off (or eroded front), underwent temperature as high as 300–320 °C. The position of the thrust front in Caledonian times located about 180 km further SE near Oslo (Fig. 1) can be used as reference for the comparison of synthetic profiles with natural data (Fig. 6).

The models proposed here focus on the effect of initial geometry and convergence rate as well as duration of extensional reactivation (Table 3).

The comparison of synthetic profiles computed in this study with the natural RSCM temperature profile allows us to constrain the most probable geometry and history for the JBT, and to discuss implications for the behaviour of crustal scale thrust zones. If the present-day down-dip length of the JBT is considered as representative for its active stage, i.e. no stretching occurred during exhumation, then the reference model $v1\alpha20$, reaching 45 km and 500 °C at 130 km along dip from front, yield a too steep thermal envelope to reproduce the natural data (Fig. 6). Profile deduced from $v1\alpha10\beta45$ yield a less steep profile and the pinning depth at 45 km is reached at 500 °C but its length remains too short to fit natural data. Models with a higher velocity (i.e. 2 cm yr^{-1}) and lower dip value (10°) better reproduce the natural data. Extensional reactivation modifies the thermal envelope only in the shallowest levels, so that no natural data can be used to discriminate between 5 or 10 Myr extension scenarios. Longer extension duration (as in $v2\alpha10L$) would have had an impact on the sampled portion of the JBT, and seem therefore unlikely.

If exhumation of the alum shale is associated with thinning and stretching along the JBT, then the present-day length of the profile can be restored to a shorter length. It can be superimposed to the reference model $v1\alpha20$ if reduced to half its length, i.e. if stretching factor during exhumation was equal to 2 (Fig. 6). Assuming such a stretching implies that the distance between the front and the thrust segment sampled in this study was also shorter (i.e. data must be shifted horizontally in Fig. 6), which is unlikely since Caledonian extension was not recorded in basement units between the Caledonian thrust front and the present-day hanging wall cut-off, the limited extensional features being locally related to Permian rifting (Sundvoll and Larsen, 1994). Even if stretching may have occurred in the JBT footwall during late Caledonian extension, it must have remained limited; $v2\alpha10$ model therefore remains our preferred simulation.

Estimate of denudation for a 10° dip thrust yields 25 km above the present-day hanging-wall cut off, which encompasses both tectonic thinning during late Caledonian extension and subsequent erosion. In the $v2\alpha10$ model only 10 km are related to extensional reactivation and 15 km have to be accommodated by post-Caledonian erosion. Independent estimates of erosion by isostatic considerations (Nielsen et al., 2009) give a 10–20 km erosion for the reduction of an initial 3500 m topography. Even if this value is more relevant for the axial domain of the mountain range, it gives a compatible upper bound for the denudation aplomb to present-day hanging-wall cut-off.

The best-fit model convergence rate value (2 cm yr^{-1}) remains low regard to the 8–10 cm yr^{-1} latitudinal relative movement deduced from palaeomagnetism for Laurentia and Baltica (Torsvik et al., 1996). A higher convergence rate, not tested in our models, would imply a shallower dip and be geometrically impossible along dip length for the JBT. The apparent discrepancy between palaeomagnetic studies and the present conclusions can be explained by (1) a possible partition of convergence on different horizontal shortening structures, the JBT being one of them, and/or (2) an actually low orthogonal convergence rate between Laurentia and Baltica, due to oblique relative motion. Rotation data from palaeomagnetism indeed indicate that Laurentia and Baltica margins trended N–S when facing each other on the equator in Silurian times (Torsvik et al., 1996), the 8–10 cm yr^{-1} latitudinal relative motion being then the strike-slip component of their bulk relative velocity. A third possibility not accounted for in the averaged convergence data based on palaeomagnetic data is that the convergence rate drastically retarded after continent–continent collision started in the Middle to Late Silurian.

Comparison of our results with other thermo-kinematic models for the Caledonides (Kylander-Clark et al., 2009, Fig. 7) show drastic discrepancy, mainly due to the higher dip (45°) used in their models. Designed to reproduce the thermal field at depth, those models did not intend to reproduce a realistic wedge structure for the upper levels, and yield unrealistic high thermal profiles for the first kilometers of the thrust interface.

Comparison with other models for thrust zones with similar size and offset to the JBT, allow a discussion of the thermal behaviour of the Scandian thrust wedge with regard to present-day analogues. JBT indeed compares in geometry and thermal state with what is inferred from PT history of the exhumed Lesser Himalayas (Beyssac et al., 2004) or what indirect imaging assess for the present-day MHT. The anisotropic interface interpreted as the MHT in P-wave amplitude tomography (Schulte-Pelkum et al., 2005) indeed flattens at 42–45 km depth 230 km north to the MBT. Hi-Climb profile (Nábělek et al., 2009) also reveals flattening of the MHT at 40 km depth 200 km north to the MFT. Thermo-kinematic modelling of temperature field in the orogenic wedge constrained by gravity data (Hetényi et al., 2007) yield a MHT reaching 520 °C at 42 km depth 190 km north to the MBT.

The best-fit thermo-kinematic model for the MHT (model 1, Henry et al., 1997) compares with the $v1\alpha20$ model for the JBT, only valid for an unlikely and considerable stretching of the alum shales. The natural data from the JBT present-day front are still about 100 °C colder (Fig. 7) than the coldest model considered in Henry et al. (1997), with moderate erosion and friction on fault implemented. Equivalent models could also be proposed for the JBT with *ad hoc* erosion rate counterbalanced by significant shear heating on fault plane. RSCM data from Devonian supra-detachment basins in the WGR, above the western continuation of the JBT: the Nordfjord Sogn Detachment, shows that a temperature anomaly of 50 to 100 °C at the base of the basins could be due to shear heating on the detachment fault system during extensional reactivation (Souche et al., 2012). Whatever the combination of competing processes, such as erosion and shear heating, Scandian orogenic wedge must have remained relatively cold throughout the complete activation sequence of the JBT, compared to MHT for instance, implying that the Caledonides would plot out of the small/cold–large/hot trend inferred from worldwide considerations on orogens (Beaumont et al., 2006). First order control of the thermal gradient along the thrust being the initial geotherm within the thrust hanging-wall combined with thrust rate, this implies or (1) that the basement units involved in the Middle Allochthon nappe sequence were relatively cold at the onset of thrusting or (2) that the JBT had a significantly higher thrust rate than the present-day MHT. This second deduction is not supported by scatter of radiochronological data from WGR eclogites buried to UHP during the same event implying a slow rate for the coeval continental subduction (Kylander-Clark et al., 2009).

6. Conclusion

The RSCM data presented here constitute the first down-dip temperature mapping across a significant part (150 km) of a crustal-scale collisional thrust zone. The JBT, that compares in size, structural position and offset with the Himalayan MHT (Labrousse et al., 2010) is developed within the Cambro-Ordovician carbon-rich alum shale, which recorded the thermal evolution of the JBT throughout the Scandian thrusting and the subsequent extensional reactivation. Peak temperature estimates in the alum shale yield peak isotherms roughly parallel to the Caledonian nappe front grading from 320 °C on its leading edge to 500 °C on its trailing edge. Based on independent estimate of maximum burial depth recorded in the alum shales (45 km see above), time constraints on the Scandian collision, and compatible convergence rates, thermo-kinematic modelling of the JBT allows us to assess its most probable geometry while active. A 10° dip toward the NW and 2 cm yr^{-1} thrust rate is the best fit with a dynamic model for the JBT, however, without considering erosion and shear heating. The preferred geometry and thrust rate are compatible with independent constraints for the Caledonian orogenic wedge and reveal cold thermal regime for the Scandian collision when compared to the Himalayan collision. This is also supported by the lack of syn-collision granites similar to the Himalayan leucogranites on the Scandinavian side of the Caledonides. The thrust rate is considerably lower than relative plate-motion velocity between Baltica and Laurentia deduced from palaeomagnetic data (Torsvik et al., 1996), implying that the JBT only accommodated part of the horizontal shortening, alternatively that the plate convergence slowed down after continent–continent collision took place. The fully thermo-mechanical modelling of the Scandian continental collision now thermally exceptionally well constrained from near the top (250 °C) to bottom (800 °C in the UHP cores of the WGR, Hacker et al., 2010), would allow to precise whether this collision remained cool due to the implication of initially cold continental margins or due to high convergence rate compared to present-day equivalents.

Appendix A. Supplementary material

Supplementary material related to this article can be found online at http://dx.doi.org/10.1016/j.epsl.2013.10.038.

References

Aldridge, A.J., 1984. Thermal metamorphism of the Silurian strata of the Oslo region, assessed by conodont colour. Geol. Mag. 121, 347–349.

Andersen, T.B., 1998. Extensional tectonics in the Caledonides of southern Norway, an overview. Tectonophysics 285, 333–351.

Andersen, T.B., Berry IV, H.N, Lux, D.R., Andresen, A., 1998. The tectonic significance of pre-Scandian ^{40}Ar/^{39}Ar phengite cooling ages in the Caledonides of western Norway. J. Geol. Soc. (Lond.) 155, 297–309.

Andersen, T.B., Corfu, F., Labrousse, L., Osmundsen, P.T., 2012. Evidence for hyperextension along the pre-Caledonian margin of Baltica. J. Geol. Soc. 169, 601–612.

Andersen, T.B., Hartz, E., Torsvik, T.H., Osmundsen, P.T., Andresen, A., Eide, E.A., Braathen, A., 2002. The aftermath of the Caledonian continental collision in the North Atlantic Region: A structural template for later events?. In: Abstracts and Proceedings of the Norwegian Geological Society, vol. 2, pp. 12–14.

Andersen, T.B., Jamtveit, B., 1990. Uplift of deep crust during orogenic extensional collapse: a model based on field studies in the Sogn-Sunnfjord region of Western Norway. Tectonics 9, 1097–1111.

Andersen, T.B., Skjerlie, K.P., Furnes, H., 1990. The Sunnfjord Melange, evidence of Silurian ophiolite accretion in the West Norwegian Caledonides. J. Geol. Soc. 147, 59–68.

Andersen, T.B., Torsvik, T.H., Eide, E.A., Osmundsen, P.T., Faleide, J.I., 1999. Permian and Mesozoic faulting in central south Norway. J. Geol. Soc. 156, 1073–1080.

Beaumont, C., Nguyen, M.H., Jamieson, R.A., 2006. Crustal flow modes in large hot orogens. Geol. Soc. (London), Spec. Publ. 268, 91–145.

Beyssac, O., Bollinger, L., Avouac, J.-P., Goffé, B., 2004. Thermal metamorphism in the Lesser Himalaya of Nepal determined from Raman spectroscopy of carbonaceous material. Earth Planet. Sci. Lett. 225, 233–241.

Beyssac, O., Goffé, B., Chopin, C., Rouzaud, J.N., 2002. Raman spectra of carbonaceous material in metasediments: a new geothermometer. J. Metamorph. Geol. 20, 859–871.

Beyssac, O., Goffé, B., Petitet, J.P., Froigneux, E., Moreau, M., Rouzaud, J.N., 2003. On the characterization of disordered and heterogeneous carbonaceous materials using Raman spectroscopy. Spectrochim. Acta 59, 2267–2276.

Bockelie, J.F., Nystuen, J.P., 1985. The southeastern part of the Scandinavian Caledonides. In: Gee, D.G., Sturt, B.A. (Eds.), The Caledonide Orogen: Scandinavia and Related Areas, vol. 1. Wiley & Sons, pp. 69–88.

Bollinger, L., Avouac, J.-P., Beyssac, O., Catlos, E.J., Harrison, T.M., Grove, M., Goffé, B., Sapkota, S., 2004. Thermal structure and exhumation history of the Lesser Himalaya in central Nepal. Tectonics 23.

Bollinger, L., Henry, P., Avouac, J.-P., 2006. Mountain building in the Nepal Himalaya: Thermal and kinematic model. Earth Planet. Sci. Lett. 244, 58–71.

Boyer, S.E., Elliott, D., 1982. Thrust systems. Am. Assoc. Pet. Geol. Bull. 66, 1196–1230.

Brueckner, H.K., van Roermund, H., 2004. Dunk tectonics: A multiple subduction/eduction model for the evolution Scandinavian Caledonides. Tectonics 23.

Bruton, D.L., Gabrielsen, R.H., Larsen, B.T., 2010. The Caledonides of the Oslo Region, Norway: stratigraphy and structural elements. Norwegian J. Geol. 90.

Bruton, D.L., Harper, D.A.T., Repetski, J.E., 1989. Stratigraphy and fauna of the Parautochthon and Lower Allochthon of southern Norway. In: Gayer, R.A. (Ed.), The Caledonian Geology of Scandinavia. Graham & Tretman, London, pp. 231–241.

Bryhni, I., Sturt, B.A., 1985. Caledonides of southeastern Norway. In: Gee, D.G., Sturt, B.A. (Eds.), The Caledonide Orogen: Scandinavia and Related Areas, vol. 1. J. Wiley and Sons, pp. 89–107.

Corfu, F., Gerber, M., Andersen, T.B., Torsvik, T.H., Ashwal, L.D., 2011. Age and significance of Grenvillian and Silurian orogenic events in the Finnmarkian Caledonides, northern Norway. Can. J. Earth Sci. 48, 419–440.

Corfu, F., Torsvik, T.H., Andersen, T.B., Ashwal, L.D., Ramsay, D.M., Roberts, R.J., 2006. Early Silurian mafic–ultramafic and granitic plutonism in contemporaneous flysch, Magerøy, northern Norway: U–Pb ages and regional significance. J. Geol. Soc. (Lond.) 163, 291–301.

Duprat-Oualid, S., Yamato, P., Pitra, P., in press. Major role of shear heating in intracontinental inverted metamorphism: Inference from a thermo-kinematic parametric study. Tectonophysics, http://dx.doi.org/10.1016/j.tecto.2013.07.037.

Fossen, H., 1992. The role of extensional tectonics in the Caledonides of South Norway. J. Struct. Geol. 14, 1033–1046.

Fossen, H., 2010. Extensional tectonics in the North Atlantic Caledonides: a regional view. Geol. Soc. (London), Spec. Publ. 335, 767–793.

Fossen, H., Dunlap, W.J., 1998. Timing and kinematics of Caledonian thrusting and extensional collapse, southern Norway: Evidence from ^{40}Ar/^{39}Ar thermochronology. J. Struct. Geol. 20.

Fossen, H., Hurich, C., 2005. The Hardangerfjord Shear Zone in SW Norway and the North Sea: a large-scale low-angle shear zone in the Caledonian crust. J. Geol. Soc. (Lond.) 162, 675–687.

Furnes, H., Skjerlie, K.P., Pedersen, R.B., Andersen, T.B., Stillman, C.J., Suthren, R.J., Tysseland, M., Garmann, L., 1990. The Solund-Stavfjord Ophiolite Complex and associated rocks, west Norwegian Caledonides – geology, geochemistry and tectonic environment. Geol. Mag. 127, 209–224.

Gabrielsen, R.H., Braathen, A., Olesen, O., Faleide, J.I., Kyrkjebø, R., Redfield, T.F., 2005. Vertical movements in south-western Fennoscandia: a discussion of regions and processes from the Present to the Devonian. In: Wandas, B. (Ed.), Onshore-Offshore Relationships on the North Atlantic Margin. In: NPF Spec. Publ., vol. 12. Elsevier, Amsterdam.

Gautneb, H., Saether, O.M., 2009. A compilation of previously published geochemical data on the lower Cambro-Silurian sedimentary sequence, including the alum shales in the Oslo region. Report No. 2009.053, Trondheim, p. 25.

Gee, D.G., 1975. A tectonic model for the central part of the Scandinavian Caledonides. Am. J. Sci. 275A, 468–515.

Gerya, T., 2010. Introduction to Numerical Geodynamic Modelling. Cambridge University Press. 358 pp.

Glodny, J., Kuhn, A., Austrheim, H., 2008. Geochronology of fluid-induced eclogite and amphibolite metamorphic reactions in a subduction–collision system, Bergen Arcs, Norway. Contrib. Mineral. Petrol. 156, 27–48.

Hacker, B.R., 2007. Ascent of the ultrahigh-pressure Western Gneiss region, Norway. In: Cloos, M., Carlson, W.D., Gilbert, M.C., Liou, J.G., Sorensen, S.S. (Eds.), Convergent Margin Terranes and Associated Regions: A Tribute to W.G. Ernst. In: Spec. Pap., Geol. Soc. Am., vol. 419. Geological Society of America.

Hacker, B.R., Andersen, T.B., Johnston, S., Kylander-Clark, A.R.D., Peterman, E.M., Walsh, E.O., Young, D., 2010. High-temperature deformation during continental-margin subduction & exhumation: The ultrahigh-pressure Western Gneiss Region of Norway. Tectonophysics 480, 149–171.

Henry, P., Le Pichon, X., Goffé, B., 1997. Kinematic, thermal and petrological model of the Himalayas: constraints related to metamorphism within the underthrust Indian crust and topographic elevation. Tectonophysics 273, 31–56.

Hetényi, G., Cattin, R., Brunet, F., Bollinger, L., Vergne, J., Nábělek, J.L., Diament, M., 2007. Density distribution of the India plate beneath the Tibetan plateau: Geophysical and petrological constraints on the kinetics of lower-crustal eclogitization. Earth Planet. Sci. Lett. 264, 226–244.

Hetényi, G., Cattin, R., Vergne, J., Nábělek, J.L., 2006. The effective elastic thickness of the India Plate from receiver function imaging, gravity anomalies and thermomechanical modelling. Geophys. J. Int. 167, 1106–1118.

Holland, T.J.B., Powell, R., 1998. An internally consistent thermodynamic data set for phases of petrological interest. J. Metamorph. Geol. 16, 309–343.

Huw Davies, J., 1999. Simple analytic model for subduction zone thermal structure. Geophys. J. Int. 139, 823–828.

Huw Davies, J., Stevenson, D.J., 1992. Physical model of source region of subduction zone volcanics. J. Geophys. Res. 97, 2037, http://dx.doi.org/10.1029/91JB02571.

Jolivet, L., Raimbourg, H., Labrousse, L., Avigad, D., Leroy, Y., Austrheim, H., Andersen, T.B., 2005. Softening triggered by eclogitization, the first step toward exhumation during continental subduction. Earth Planet. Sci. Lett. 237, 532–547.

Kirkland, C.L., Daly, J.S., Whitehouse, M.J., 2008. Basement-cover relationships of the Kalak Nappe Complex, Arctic Norwegian Caledonides and constraints on Neoproterozoic terrane assembly in the North Atlantic Region. Precambrian Res. 160, 245–276.

Krogh, T.E., Kamo, S.L., Robinson, P., Terry, M.P., Kwok, K., 2011. U–Pb zircon geochronology of eclogites from the Scandian Orogen, northern Western Gneiss Region, Norway: 14–20 million years between eclogite crystallization and return to amphibolite-facies conditions. Can. J. Earth Sci. 48, 441–472.

Kylander-Clark, A.R.D., Hacker, B.R., Johnson, C.M., Beard, B.L., Mahlen, N.J., 2009. Slow subduction of a thick ultrahigh-pressure terrane. Tectonics 28, http://dx.doi.org/10.1029/2007TC002251.

Kylander-Clark, A.R.D., Hacker, B.R., Mattinson, J.M., 2008. Slow exhumation of UHP terranes: Titanite and rutile ages of the Western Gneiss Region, Norway. Earth Planet. Sci. Lett. 272, 531–540.

Labrousse, L., Hetényi, G., Raimbourg, H., Jolivet, L., Andersen, T.B., 2010. Initiation of crustal-scale thrusts triggered by metamorphic reactions at depth: insights from a comparison between the Himalayas and Scandinavian Caledonides. Tectonics 29, http://dx.doi.org/10.1029/2009TC002602.

Lahfid, A., Beyssac, O., Deville, E., Negro, F., Chopin, C., Goffé, B., 2010. Evolution of the Raman spectrum of carbonaceous material in low-grade sediments of the Glarus Alps (Switzerland). Terra Nova 22, 354–360.

Lundmark, A.M., Corfu, F., 2007. Age and origin of the Ardal dike complex, SW Norway: False isochrons, incomplete mixing and the origin of Caledonian granites in basement nappes. Tectonics TC2007.

Lutro, O., Tveten, E., 1998. Geologisk kart over Noreg. Årdal, Norges geologiske undersøking.

Milnes, A.G., Wennberg, O.P., Skår, Ø., Koestler, A.G., 1997. Contraction, extension and timing in the South Norwegian Caledonides: the Sognefjord transect. In: Burg, J.-P., Ford, M. (Eds.), Orogeny Through Time. In: Geol. Soc. Spec. Publ., vol. 121, pp. 123–148.

Morley, C.K., 1986. The Caledonian thrust front and palinspastic restorations in the southern Norwegian Caledonides. J. Struct. Geol. 8, 753–765.

Nábělek, J.L., Hetényi, G., Vergne, J., Sapkota, S., Kafle, B., Jiang, M., Su, H., Chen, J., Huang, B.S., 2009. Underplating in the Himalaya? Tibet collision zone revealed by the Hi-CLIMB experiment. Science 325, 1371–1374.

Nielsen, S.B., Gallagher, K., Leighton, C., Balling, N., Svenningsen, L., Holm Jacobsen, B., Thomsen, E., Nielsen, O.B., Heilman-Clausen, C., Egholm, D.L., Summerfield, M.A., Clausen, O.R., Piotrowski, J.A., Thorsen, M.R., Huuse, M., Abrahamsen, N., King, C., Lykke-Andersen, H., 2009. The evolution of western Scandinavian topography: A review of Neogene uplift versus the ICE (isostasy-climate-erosion) hypothesis. J. Geodyn. 47, 72–95.

Nystuen, J.P., 1981. The Late Precambrian Sparagmites of Southern-Norway – a Major Caledonian Allochthon – the Osen-Roa Nappe complex. Am. J. Sci. 481, 69–94.

Nystuen, J.P., Andresen, A., Kumpulainen, R.A., Siedlecka, A., 2008. Neoproterozoic basin evolution in Fennoscandia, East Greenland and Svalbard. Episodes 31, 35–43.

Oftedahl, C., 1943. Overskyvninger i den norsk fjellkjede. Naturen (Osio) 5, 243–250.

Redfield, T.F., Osmundsen, P.T., Hendriks, B.W.H., 2005. The role of fault reactivation and growth in the uplift of western Fennoscandia. J. Geol. Soc. 162, 1013–1030.

Roberts, D., 2003. The Scandinavian Caledonides: event chronology, palaeogeographic settings and likely modern analogues. Tectonophysics 365, 283–299.

Roberts, D., Gee, D.G., 1985. An introduction to the structure of the Scandinavian Caledonides. In: Gee, D.G., Sturt, B.A. (Eds.), The Caledonide Orogen: Scandinavia and Related Areas, vol. 1. J. Wiley, Chichester, pp. 55–68.

Root, D., Corfu, F., 2012. U–Pb geochronology of two discrete Ordovician high-pressure metamorphic events in the Seve Nappe Complex, Scandinavian Caledonides. Contrib. Mineral. Petrol. 163, 769–788.

Royden, L., 1993. The steady-state thermal structure of eroding orogenic belts and accretionary prisms. J. Geophys. Res. 98, 4487–4507.

Rudnick, R.L., Gao, S., 2003. The composition of the continental crust. In: Rudnick, R.L. (Ed.), The Crust. In: Treatise Geochem., vol. 3. Elsevier–Pergamon, Oxford, pp. 1–64.

Schulte-Pelkum, V., Monsalve, G., Sheehan, A., Pandey, M.R., Sapkota, S., Bilham, R., 2005. Imaging the Indian subcontinent beneath the Himalayas. Nature 435, 1222–1225.

Souche, A., Beyssac, O., Andersen, T.B., 2012. Thermal structure of supra-detachment basins: a case study of the Devonian basins of western Norway. J. Geol. Soc. 169, 427–434.

Souche, A., Medvedev, S., Andersen, T.B., Dabrowski, M., 2013. Shear heating in extensional detachments: implications for the thermal history of the Devonian basins of W Norway. Tectonophysics 365, 283–299.

Sundvoll, B., Larsen, B.T., 1994. Architecture and early evolution of the Oslo Rift. Tectonophysics 240, 173–189.

Torsvik, T.H., Cocks, L.R.M., 2005. Norway in space and time: A Centennial cavalcade. Norwegian J. Geol. 85, 73–86.

Torsvik, T.H., Smethurst, M.A., Meert, J.G., van der Voo, R., McKerrow, W.S., Brasier, M.D., Sturt, B.A., Walderhaug, H.J., 1996. Continental break-up and collision in the Neoproterozoic and Palaeozoic – A tale of Baltica and Laurentia. Earth-Sci. Rev. 40, 229–258.

Zhao, W., Nelson, K.D., Team, P.I., 1993. Deep seismic reflection evidence for continental underthrusting beneath southern Tibet. Nature 366, 557–559.